

HT2007-32916

THE EFFECTS OF INLET FLOW CONDITIONS ON GAS-LIQUID TWO-PHASE FLOW IN A MICRO TUBE

Shota Hayashi

Dept. of Mech. Eng., The Univ. of Tokyo
Hongo 7-3-1, Bunkyo-ku, Tokyo 113-8656, Japan
hayashi@thtlab.t.u-tokyo.ac.jp

Nobuhide Kasagi

Dept. of Mech. Eng., The Univ. of Tokyo
Hongo 7-3-1, Bunkyo-ku, Tokyo 113-8656, Japan
kasagi@thtlab.t.u-tokyo.ac.jp

Yuji Suzuki

Dept. of Mech. Eng., The Univ. of Tokyo
Hongo 7-3-1, Bunkyo-ku, Tokyo 113-8656, Japan
ysuzuku@thtlab.t.u-tokyo.ac.jp

ABSTRACT

In the present study, the effects of inlet geometry on the microscale two-phase flow patterns have been examined. The relationships among the flow pattern, the void fraction, the pressure loss and the heat transfer coefficient have been also investigated under different inlet flow conditions. At the inlet, a stainless steel tube is inserted into the micro glass tube, of which inner diameter is 300 and 600 μm . The gas and liquid paths and the diameter of the inner tube are interchangeable. The flow patterns are recorded at the inlet and also in the developed region in the micro tubes. The flow patterns observed in the 600 μm tube are bubbly, slug, churn and annular flows, while bubbly and churn flows are not present in the 300 μm tube. For bubbly and slug flows, bubble formation process is found to be strongly affected by the inlet conditions. Accordingly, the pressure loss as well as the heat transfer rate are changed. In addition, the bubble size is not uniquely determined; bubbles of different sizes are observed in repeated experiments under the same inlet flow conditions. On the other hand, for churn and annular flows, the flow patterns are not affected by the inlet conditions.

Keywords: gas-liquid two-phase flow, microchannel, inlet geometry, flow pattern, pressure drop, heat transfer

INTRODUCTION

Gas-liquid two-phase flow in a micro conduit has become very important in many emerging applications such as micro heat exchangers and Lab-on-a-chip. In order to

successfully design these devices, understanding of flow physics in micro scale is crucial.

It is well known that gas-liquid two-phase flows in microchannels exhibit different behavior as compared to that formed in macro-sized channels. For example, Yen et al. (2003) observed up to 70 K liquid superheat over the saturation temperature in their 0.19 mm ID tube. They also found that the heat transfer coefficient is independent on the mass and heat fluxes. Kawahara et al. (2002) and Chung et al. (2004) investigated the adiabatic two-phase flow in tubes of 50 ~ 250 μm diameter and reported that significant differences in the flow regime maps and void fraction from those for minichannels with diameters above ~ 1 mm have been observed. Furthermore, Kawaji et al. (2005) showed that the inlet geometry played an important part to the characteristics of adiabatic gas-liquid two-phase flow in microchannels.

In order to better understand convective boiling heat transfer in microchannels, it is necessary to clarify the heat transfer characteristics of gas-liquid two-phase flow without phase change. To the best of our knowledge, such investigation is not available in literature, although Monde et al. (1995) have reported that heat transfer could be enhanced by passing of bubbles in a narrow rectangular channel.

The main objective of this work is to clarify the process on formation of various flow patterns as well as the effect of inlet flow conditions on the flow patterns. Furthermore, the relationships among the flow pattern, the void fraction, the pressure loss and the heat transfer coefficient are to be investigated under different inlet flow conditions.

NOMENCLATURE

A	cross-sectional area of tube, m^2
C_p	specific heat, $J/(g\ K)$
C	Chisholm parameter
d	inner diameter of tube, m
h	heat transfer coefficient, $W/(m^2\ K)$
I	electric current, A
j	superficial velocity, $m/s (= Q/A)$
l	length, m
Nu	Nusselt number $(= hd/\lambda)$
p	pressure, Pa
q	heat flux, J/m^2
Q	volumetric flow rate, m^3/s
Re	superficial Reynolds number $(= \rho jd/\mu)$
T	local temperature, K
U	mean velocity, m/s
V	voltage, V
X	Martinelli parameter

Greek Symbols

α	void fraction
β	volumetric gas flow ratio
Φ_L^2	two-phase friction multiplier
λ	thermal conductivity, $W/(m\ K)$
μ	viscosity, $Pa\ s$
ρ	density, kg/m^3

Subscripts

<i>ambi</i>	ambient
<i>bulk</i>	bulk-mean
<i>G</i>	gas phase
<i>in</i>	inner
<i>L</i>	liquid phase
<i>out</i>	outer
<i>TP</i>	two-phase

EXPERIMENTAL APPARATUS

Experiments were carried out under both adiabatic and heating conditions. The void fraction and the pressure loss were measured in adiabatic experiment, while the heat transfer coefficient in heating experiment. Experimental setup except for test section is the same for both experiments.

Experimental Setup and Condition

Figure 1 shows the experimental setup used in the adiabatic experiment. Distilled water and nitrogen were used as liquid and gas phases, respectively. The liquid flow rate and the gas flow rate were controlled by a twin plunge pump (GL sciences, PU714) and a mass flow controller (KOFLOC, Model3200), respectively. For visualization of flow patterns, micro glass tubes of 300 and 600 μm have been used for test section. The inlet condition was provided by concentric tubes. At the inlet, a stainless steel tube was inserted into the micro tube as shown in Fig. 2. Gas was introduced into the inner pipe, while liquid was introduced into the outer annular section. The gas and liquid paths were interchangeable. The diameter of the inner tube was also changed. Table 1 shows the experimental conditions in the adiabatic experiments. The gas superficial velocity is the value at atmospheric pressure.

Figure 3 shows the test section used in the heating experiments. A mixture of ITO and silver was evenly sputtered on the outer surface of the glass tube for the heating element. Four K-type thermocouples of 25 μm OD, calibrated with the accuracy of 0.1 K, were attached on the tube outer surface with thermally conductivity silicon. Table 2 shows the experimental conditions in the heating experiments.

A high-speed camera (Vision Research, Phantom v5) was employed for recording visualized flow patterns inside the micro tube. Each image was formed by 1024 x 128 pixels and the frame rate was 1000–4000 frames/sec.

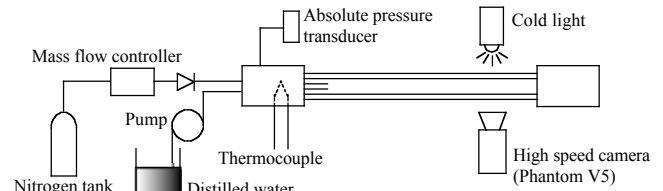


Fig. 1 Experimental setup for adiabatic experiment

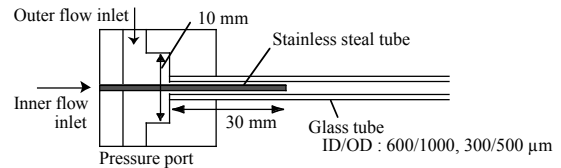


Fig. 2 Inlet geometry

Table 1 Experimental conditions in adiabatic experiments

d [μm]	Inner tube (ID/OD) [μm]	Inner path	j_L [m/s]	j_G [m/s]	Re_L	Re_G
600	100/200	Gas	0.05-0.5	0.11-6.4	30-300	4.6-274
600	300/400	Gas	0.05-0.5	0.11-6.4	30-300	4.6-274
600	300/400	Liquid	0.05-0.3	0.11-6.4	30-180	4.6-274
300	150/200	Gas	0.03-0.15	0.33-21	9-45	7-465
300	150/200	Liquid	0.05, 0.1	0.33-21	15, 30	7-465

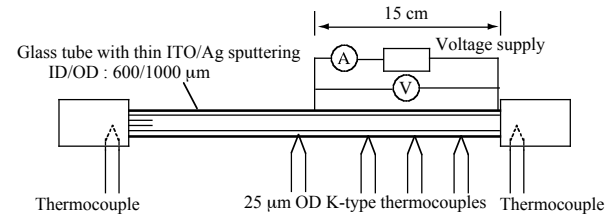


Fig. 3 Test section for heating experiment

Table 2 Experimental conditions in heating experiments

d [μm]	Inner tube (ID/OD) [μm]	Inner path	j_L [m/s]	j_G [m/s]	q [kW/m^2]
600	300/400	Gas	0.2	0.11-6.4	18-19
600	300/400	Gas	0.3	0.11-6.4	24-26

Data Reduction

The void fraction for slug flow can be estimated by

$$\alpha = \frac{j_G}{U_G} \quad (1)$$

The gas average velocity for slug flow can be obtained from traveling distance of bubble between successive images. On the other hand, the void fraction for annular flow was not estimated, since it is difficult to measure the gas average velocity and the film thickness for annular flow.

The inlet pressure is measured at the inlet manifold located upstream the mixing region. In order to compensate the pressure loss at the inlet and the outlet, the frictional pressure loss in the micro tube is obtained with the inlet pressure for two tubes with different length, i.e.,

$$(dP/dz)_{TP} = \frac{(P_1 - P_2)}{l_1 - l_2} \quad (2)$$

where P_1 and P_2 are the inlet pressure respectively for the tube length l_1 and l_2 . For the 600 μm ID tubes, $l_1 = 40$ cm and $l_2 = 30$ cm, respectively. For the 300 μm ID tubes, $l_1 = 30$ cm and $l_2 = 15$ cm, respectively.

The heat transfer coefficient h can be estimated as

$$h = \frac{q}{T_{wall,in} - T_{bulk}} \quad (3)$$

A preliminary heating experiment with an empty test section was performed to estimate the heat loss to the surroundings. The heat flux q can be calculated as

$$q = \frac{IV}{\pi d_{in} l} - q_{loss} = \frac{IV}{\pi d_{in} l} - h_{natural} \cdot (T_{wall,out} - T_{ambi}) \frac{d_{out}}{d_{in}}, \quad (4)$$

where l is the heating length. The inner wall temperature is solved by the one-dimensional heat conduction equation in cylindrical coordinates:

$$T_{wall,in} = T_{wall,out} - \frac{q \cdot d_{in}}{2\lambda_{glass}} \ln \frac{d_{out}}{d_{in}} \quad (5)$$

The bulk-mean temperature T_{bulk} can be estimated as

$$T_{bulk} = T_{L,inlet} + \frac{\pi q \cdot d_{in} \cdot x}{Q_L \cdot C p_L}, \quad (6)$$

where x is the distance from the leading edge of the heater.

RESULTS AND DISCUSSION

Two-Phase Flow Patterns

The flow patterns are recorded with the high-speed camera at the inlet and also in the developed region in the micro glass tube. The flow patterns observed are slug, churn and annular flows in the 600 μm tube, while churn flow is not present in the 300 μm tube.

Flow pattern definition

In the present paper, the flow patterns are defined as follows:

Slug flow: The flow pattern consists of bubbles with semi-spherical caps and flat tails, which occupy the most of tube cross-section. For small flow rate, the tail is also semi-spherical. For large flow rate, the tail is disturbed. Specially, the flow with bubbles smaller than tube diameter is referred to as bubbly flow.

Transitional flow: This flow is in the transition region from slug flow to annular flow. The flow containing long bubbles with disturbed area is included in this category. The periodic flow is also included in this category, in which slug and annular flows appear alternatively.

Annular flow: The liquid flows in a thin film along the tube wall. At intervals, the liquid slugs are observed. The flow with liquid rings on the liquid film is included in this flow pattern. The flow mode where appear many liquid slugs containing many small gas bubbles is referred to as churn flow.

600 μm tube with inner tube of 100/200 μm ID/OD

For bubbly and slug flows, several mechanisms of bubble formation seem to exist, and they are dependent on the inlet flow conditions. Figure 4 shows the bubble formation processes when the inner tube ID/OD is 100/200 μm and the inner path is gas. There are three mechanisms of bubble formation.

Mechanism 1: Individual bubbles are formed in a region immediately downstream of the inner tube exit. The length of the bubble formed depends on the inlet condition.

Mechanism 2: Longer bubbles are formed by the coalescence of smaller bubbles at region immediately downstream of the inner tube exit. The length of each bubble is almost constant at a particular inlet condition.

Mechanism 3: The length of the bubble increases further through the coalescence of more smaller bubbles in the region just downstream of the inner tube exit, until it is broken by the liquid phase.

In addition, the bubble size is not uniquely determined, so that bubbles of different sizes are observed in repeated experiments under the same inlet flow conditions.

Figure 5 shows the flow patterns in the inlet region and also in the developed region. The coalescence of bubbles takes place in the region immediate downstream of the inlet. Accordingly, the bubble size depends on the initial bubble formation process. On the other hand, for transitional, churn and annular flows, the flows in the inlet region are different from those formed in the developed region. At the inlet, the gas-liquid interface is disturbed, but not so in the developed region.

Figure 6 shows the flow pattern in developed region for the large gas flow rate. For $j_L = 2.18$ m/s, in the developed region, long bubbles observed may have their origin from the coalescence of several long bubbles. The combining areas are slightly disturbed. For $j_L = 3.27$ m/s, the flow seems to be an annular flow with smooth gas-liquid interface. However, the liquid slugs are observed at intervals. For $j_L = 5.46$ m/s, liquid ring are formed on a liquid film gradually. The liquid slugs are observed at intervals, which absorb the liquid rings. And then, the liquid rings are formed again.

600 μm tube with inner tube of 300/400 μm ID/OD

Figure 7 shows the bubble formation processes in the case of the inner tube of 300/400 μm ID/OD when the inner path is either gas or liquid phase. When the inner path is gas, for almost all flow conditions, the bubble formation process is similar to that shown in Fig. 4a, i.e. mechanism 1. When the inner path is liquid, the liquid sticks to the glass tube wall initially by the surface tension in the region just downstream of the inlet. As a result, the bubble formation process is similar to mechanism 1.

Figure 8 shows the bubble size under different inlet flow conditions. For bubbly and slug flows, the bubble size is affected by the inlet geometries. Unlike the slug flow, churn and annular flows are not affected by the inlet geometries.

300 μm tube with inner tube of 150/200 μm ID/OD

For slug flow, as in the case of the 600 μm tube, several mechanisms of bubble formation seem to exist, and the bubble size is affected by the inlet geometries.

Figure 9 shows the flow pattern in the developed region when the gas flow rate is large. The annular flow patterns are similar to those in the 600 μm tube, but some differences exist. For the 300 μm tube, less liquid slugs are observed if compared with the 600 μm tube under the same superficial gas and liquid velocities. The liquid rings expanded to the liquid bridges, before they are broken down by the gas flow. In addition, the asymmetric liquid rings are sometimes observed.

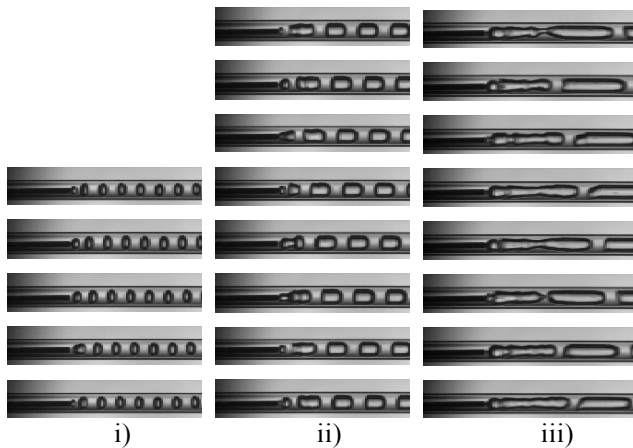


Fig. 4 Bubble formation at inlet
 $(j_L = 0.2 \text{ m/s}, 100/200(\text{gas}), \text{fps} = 2000);$
 i) $j_G = 0.11 \text{ m/s}$, ii) $j_G = 0.33 \text{ m/s}$, iii) $j_G = 1.09 \text{ m/s}$

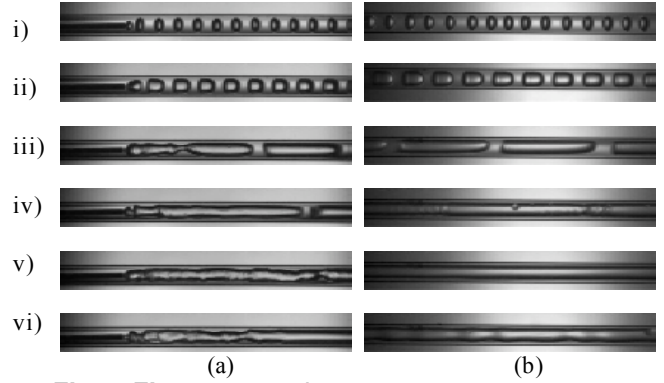


Fig. 5 Flow pattern ($j_L = 0.2 \text{ m/s}, 100/200(\text{gas})$):
 (a) inlet region, (b) developed region;
 i) $j_G = 0.11 \text{ m/s}$, ii) $j_G = 0.33 \text{ m/s}$, iii) $j_G = 1.09 \text{ m/s}$,
 iv) $j_G = 2.18 \text{ m/s}$, v) $j_G = 3.27 \text{ m/s}$, vi) $j_G = 5.46 \text{ m/s}$

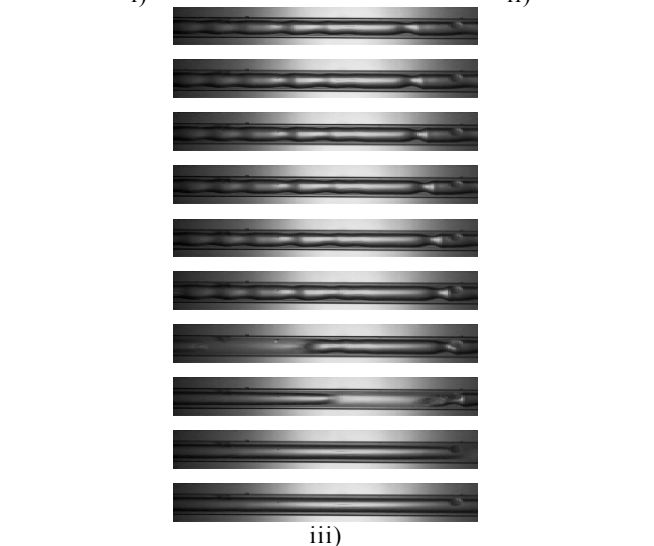
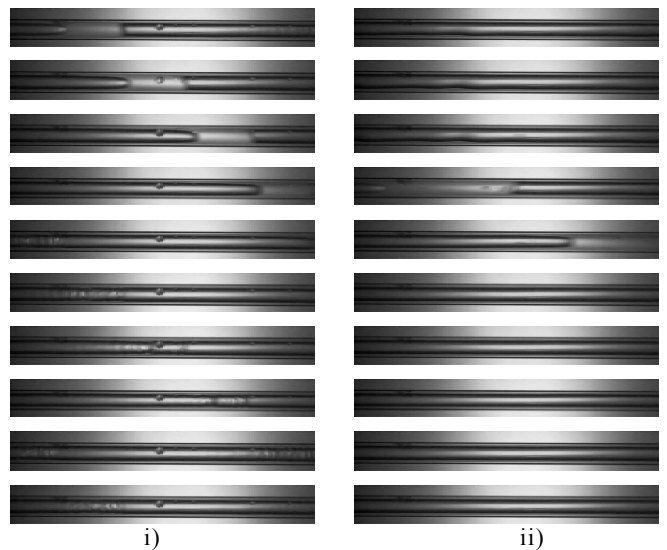


Fig. 6 Flow pattern in developed region for large gas flow rate ($j_L = 0.2 \text{ m/s}, 100/200(\text{gas}), \text{fps} = 2000$):
 i) $j_G = 2.18 \text{ m/s}$, ii) $j_G = 3.27 \text{ m/s}$, iii) $j_G = 5.46 \text{ m/s}$

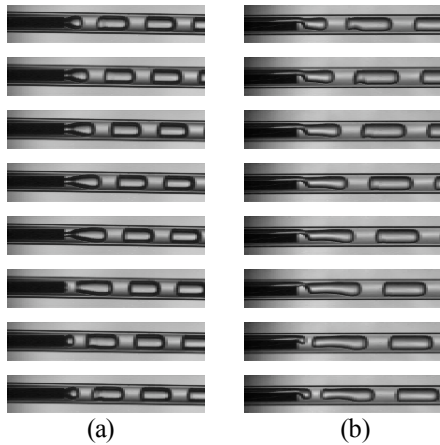


Fig. 7 Bubble formation under different inlet condition ($j_L = 0.2$ m/s, $j_G = 0.33$ m/s, fps = 2000);
(a) 300/400(gas), (b) 300/400(liquid)

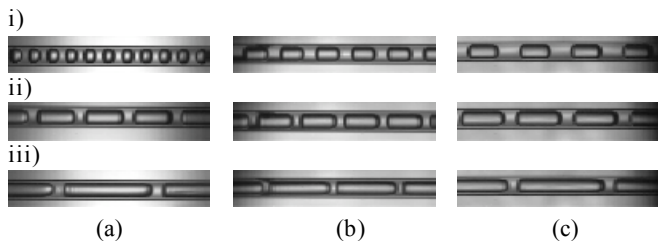


Fig. 8 Bubble size under different inlet condition ($j_L = 0.1$ m/s):
(a) 100/200(gas), (b) 300/400(gas), (c) 300/400(liquid);
i) $j_G = 0.11$ m/s, ii) $j_G = 0.33$ m/s, iii) $j_G = 0.76$ m/s

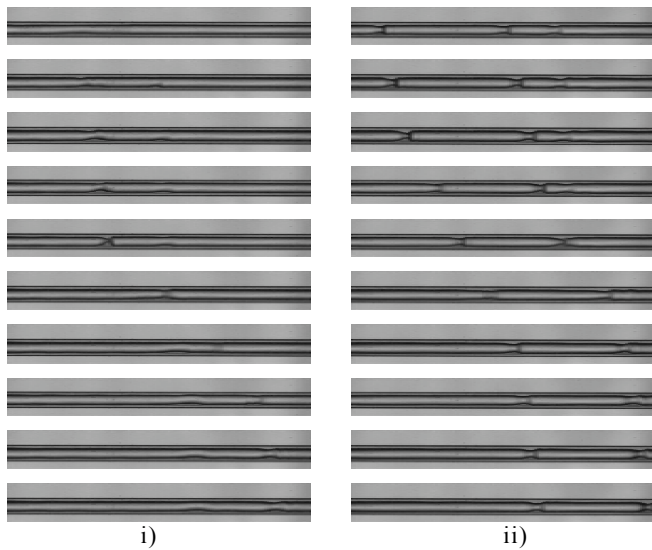


Fig. 9 Flow pattern in developed region ($j_L = 0.05$ m/s, fps = 2000);
i) $j_G = 2.18$ m/s, ii) $j_G = 5.46$ m/s

Void Fraction

Figure 10 shows the relation between the void fraction α and the volumetric gas flow ratio β defined as

$$\beta = \frac{Q_G}{Q_G + Q_L} = \frac{j_G}{j_G + j_L} = \alpha \frac{U_G}{U_{TP}} \quad (7)$$

For all conditions examined in the 600 μm tube, the experimental results are in good agreement with the estimates with the Armand correlation (Armand & Treschev, 1949), i.e.,

$$\alpha = 0.833 \times \beta = 0.833 \times \alpha \frac{U_G}{U_{TP}} \quad (9)$$

Figure 11 shows the experimental results for the slug flow in the 300 μm tube. The void fractions are in general lower than the Armand correlation. At particular volumetric gas flow ratio, the void fraction depends on the liquid superficial velocity, but independent of the path chosen for the liquid phase.

Figure 12 shows the relation between the bubble velocity $U_{Bubble}(=U_G)$ and the two-phase superficial velocity U_{TP} in the 300 μm tube. It is found that the bubble velocities are determined only by two-phase superficial velocity. Since the liquid superficial velocity is much smaller than the gas superficial velocity, it can also be interpreted that the bubble velocities are dependent on the gas superficial velocity.

Kawahara et al. (2002) reported similar disagreement in a 100 μm tube. In their experiments, however, bubbly and slug flows were absent and the void fraction was independent of the liquid velocity. Therefore, the cause of disagreement with the Armand correlation in our experiment may be different from that of Kawahara. Kawaji et al. (2005) suggested that the disagreement was due largely to the flow pattern (a gas core flow with liquid film). However, the present data also show disagreement for slug flow. Kawahara et al. introduced gas/liquid mixture into their microchannel from a large manifold. Rather long gas plugs observed might be attributed to alternate indraft of gas/liquid phases into the channel. Moreover, it is also considered that the disagreement may be attributed to the fluctuation of total flow rate caused by the alternate indraft. That is, the total flow rate becomes large because of small pressure loss when the volume of the indrafted gas is large. On the other hand, the total flow rate becomes small because of large pressure loss when the volume of the indrafted gas is small. As a result, the average gas velocity becomes larger. However, according to the present data, it is clear that the void fraction should be lower than the Armand correlation for slug flow in the 300 μm tube, even when the gas and liquid flow rates at the inlet are well determined.

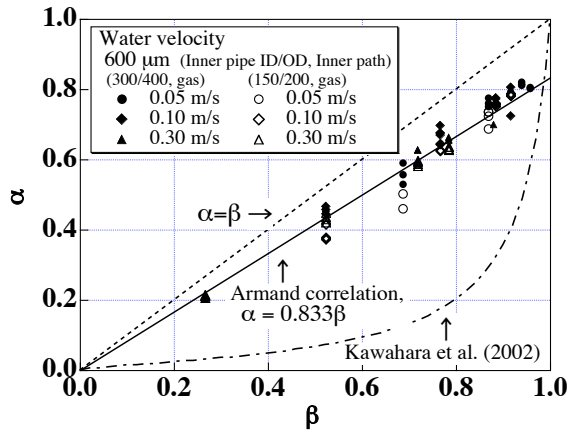


Fig. 10 Void fraction for slug flow in 600 μm tube

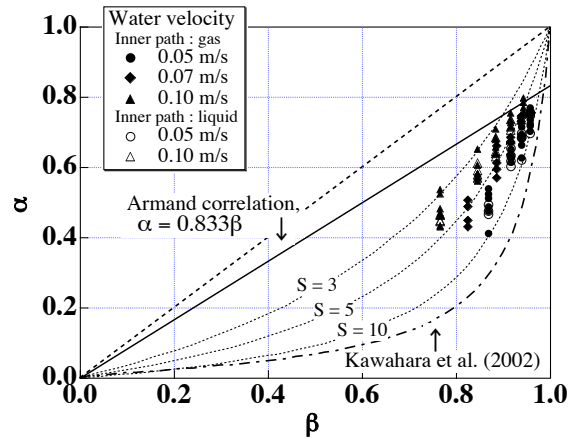


Fig. 11 Void fraction for slug flow in 300 μm tube

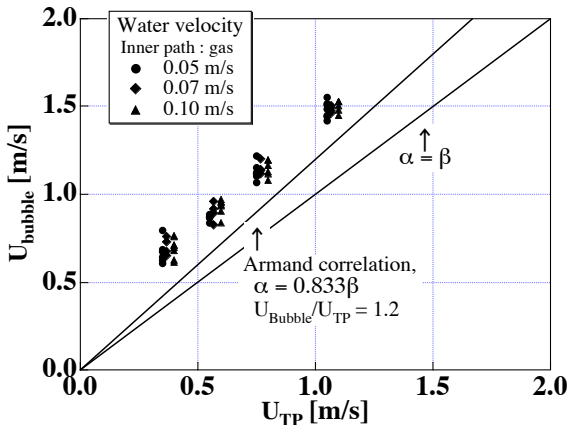


Fig. 12 Bubble velocity in 300 μm tube

Friction Pressure Loss

The frictional pressure loss is compared with the conventional correlation for macro-sized channels, i.e. the Lockhart-Martinelli model (1949). The two-phase pressure gradient is evaluated through the two-phase multiplier Φ_L^2 and the Martinelli parameter X defined respectively as

$$\Phi_L^2 = \frac{(dp/dz)_{TP}}{(dp/dz)_L}, \quad (9)$$

and

$$X^2 = \frac{(dp/dz)_L}{(dp/dz)_G}. \quad (10)$$

For macro-sized tube, the relation between Φ_L^2 and X is usually given by the Chisholm (1967) correlation, i.e.,

$$\Phi_L^2 = 1 + \frac{C}{X} + \frac{1}{X^2}, \quad (11)$$

where C is the Chisholm parameter, of which value ranges between 5 and 20; $C=5$ corresponds to the case where both phases are laminar.

Figure 13 shows the relation between Φ_L^2 and X in the 600 μm tube. For slug flows ($2 < X < 10$), the pressure loss is underestimated by the conventional correlation for macro-sized channels. However, for large liquid flow rates, the pressure loss shows relatively better agreement with the conventional correlation. For annular and churn flows ($X < 2$), the pressure loss is overestimated, and is not affected by the liquid flow rate.

Figure 14 shows the effect of inlet geometry on the pressure loss. For slug flows ($2 < X < 10$), it is found that the initial bubble length affects the pressure loss. Shorter bubble length gives larger pressure loss. For annular and churn flows ($X < 2$), the pressure loss is not affected by the inlet condition. Therefore, it is evident that the pressure loss in microchannels is largely affected by the flow pattern.

Figures 15 and 16 show the results in the 300 μm tube. The present data exhibit the same tendency as those in the 600 μm tube. The results of pressure loss reported by Kawahara et al. are much lower than the present data. It might be also attributed to alternate indraft of gas/liquid phases into the channel.

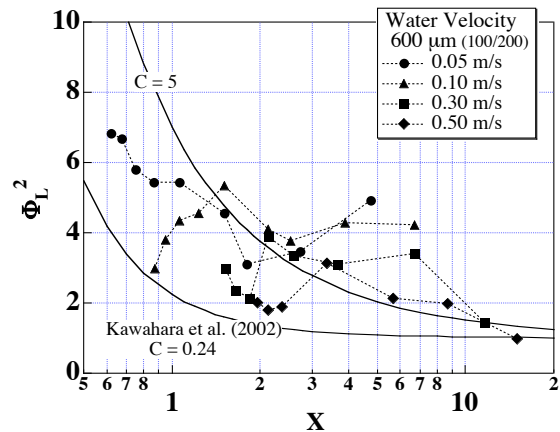


Fig. 13 Two-phase friction multiplier in 600 μm tube (effect of liquid superficial velocity)

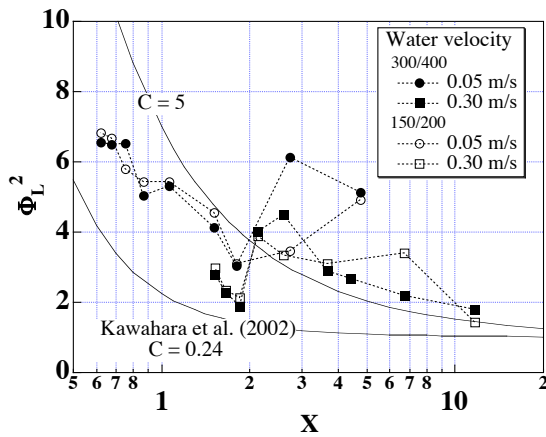


Fig. 14 Two-phase friction multiplier in 600 μm tube (effect of inlet geometry)

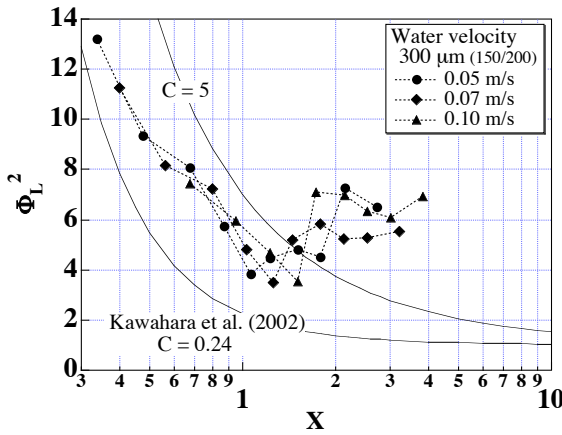


Fig. 15 Two-phase friction multiplier in 300 μm tube (effect of liquid superficial velocity)

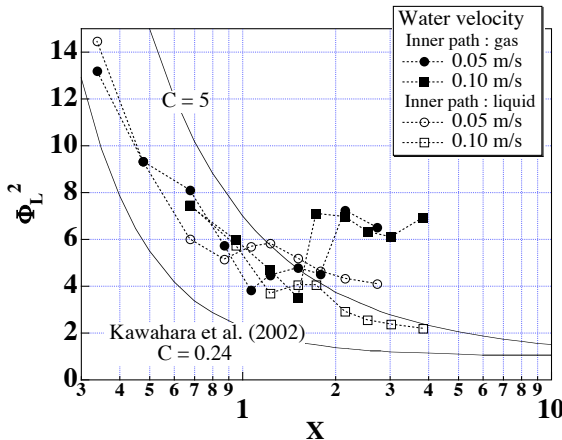


Fig. 16 Two-phase friction multiplier in 300 μm tube (effect of inlet geometry)

Heat Transfer Characteristics

Figures 17 and 18 show the temperature difference between the inner wall $T_{wall,in}$ and the liquid T_{bulk} at 39 mm from the leading edge of the heater. The uncertainty interval of every data point shown in the figure includes only the random error. The present data also include the bias error, but it is equal under the same liquid flow rate and heat flux. The Nusselt number estimated from the single-phase

experiment is 6-6.5 (theoretical value equals to 4.36), and this deviation is due to the bias error.

For slug flow, the heat transfer rate exhibits the opposite tendency from the pressure loss. Figure 19 shows the bubble sizes for different flow conditions. Increasing the gas flow rate also represents increasing the liquid velocity and enlarging the bubble size. The large liquid velocity should give the heat transfer enhancement. However, the heat transfer rate becomes smaller, that is, the long gas bubble gives smaller heat transfer rate than that of the small gas bubble. Therefore, for slug flow, it is expected that the heat transfer enhancement is attributed to the renewal of thermal layer due to the circulation in the liquid slug by passing the bubbles, and the effect of the thin film is comparatively small. Under the same gas and liquid flow rates, the effect of bubble size on the heat transfer is the same as that on the pressure loss. In addition, for $j_L = 0.3 \text{ m/s}$ and $j_G = 0.76 \text{ m/s}$, the heat transfer rate is larger than that in $j_G = 0.56$ in spite of longer bubble. It seems that the other mechanism of heat transfer exists.

On the other hand, for transition region and annular flow, the heat transfer rate denotes the same tendency as the pressure loss.

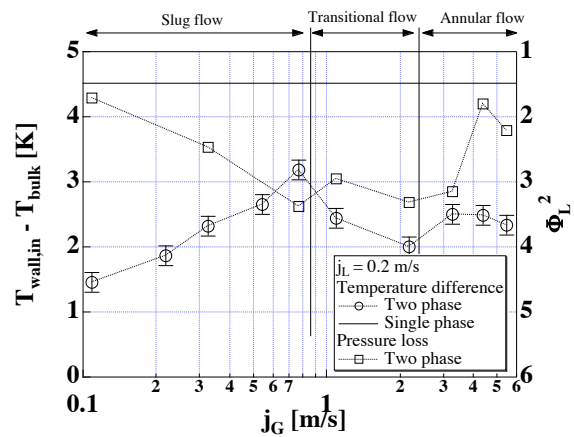


Fig. 17 Comparison between heat transfer and pressure loss for two-phase flow in 600 μm tube ($j_L = 0.2 \text{ m/s}$)

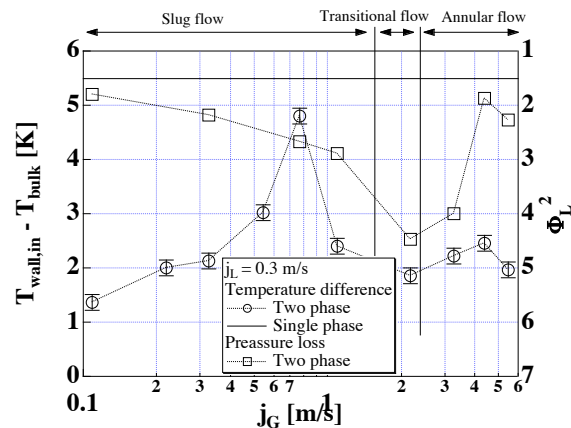


Fig. 18 Comparison between heat transfer and pressure loss for two-phase flow in 600 μm tube ($j_L = 0.3 \text{ m/s}$)

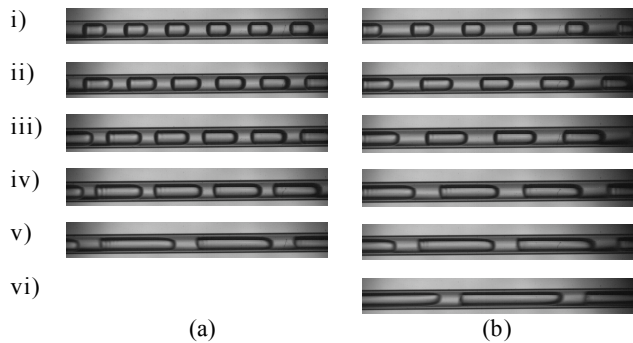


Fig. 19 Bubble size observed under different flow conditions:

(a) $j_L = 0.2$ m/s, (b) $j_L = 0.3$ m/s;
 i) $j_G = 0.11$ m/s, ii) $j_G = 0.22$ m/s, iii) $j_G = 0.33$ m/s,
 iv) $j_G = 0.56$ m/s, v) $j_G = 0.76$ m/s, vi) $j_G = 1.09$ m/s

CONCLUSIONS

The effects of inlet flow conditions on two-phase flow in micro tubes have been investigated experimentally. Under the well defined inlet flow conditions, i.e. the gas and liquid flow rate are defined at a micro tube inlet respectively, the two-phase flows are not so affected by inlet geometry. However, for slug flow, the coalescence of bubbles takes place only in the region just downstream of the inlet, so that the bubble size depends on the initial bubble formation process. Accordingly, the bubble size is affected by the inlet geometry.

Furthermore, the following conclusions are obtained for the void fraction, pressure loss and heat transfer rate.

1. For the 600 μm tube, the void fractions are in good agreement with the Armand correlation. However, for the 300 μm tube, the void fractions disagree with the Armand correlation, and are affected by the liquid velocity.
2. Unlike the conventional size, the pressure loss is not determined only by the flow rate. The pressure loss in microchannels is largely affected by the flow pattern. Specially, for slug flow, the pressure loss is largely affected by the bubble size.
3. For slug flow, the heat transfer is enhanced by the mixing effect of bubble. On the other hand, the effect of the thin

film is comparatively small unlike convective boiling heat transfer.

ACKNOWLEDGMENTS

We would like to thank Professor Naoki Shikazono and Dr. Koji Fukagata at the University of Tokyo for their fruitful discussions and advice.

REFERENCES

- [1] Yen, T.H., Kasagi, N., and Suzuki, Y., 2003, "Forced convective boiling heat transfer in microtubes at low mass and heat fluxes," *Int. J. Multiphase Flow*, **29**, pp. 1771-1792.
- [2] Kawaji, M., Mori, K., and Bolintineanu, D., 2005, "The Effects of Inlet Geometry on Gas-Liquid Two-Phase Flow in Microchannels," *Proc. 3rd Int. Conf. on Microchannels and Minichannels*.
- [3] Kawahara, A., Chung, P.M.Y., and Kawaji, M., 2002, "Investigation of Two-Phase Flow Pattern, Void Fraction and Pressure Drop in a Microchannel," *Int. J. Multiphase Flow*, **28**, pp. 1411-1435.
- [4] Chung, P.M.Y., and Kawaji, M., 2004, "The Effect of Channel Diameter on Adiabatic Two-Phase Flow Characteristics in Microchannels," *Int. J. Multiphase Flow*, **30**, pp. 735-761.
- [5] Monde, M., and Mitsutake, Y., 1995, "Enhancement of Heat Transfer due to Bubble Passing through a Narrow Vertical Rectangular Channel," *Heat Mass Transfer*, **31**, pp. 77-82.
- [6] Armand, A.A., and Treschev, G.G., 1946, "The Resistance During the Movement of A Two-Phase Systems in Horizontal Pipes," *Izv. Vses. Teplotek. Inst.*, **1**, pp. 16-23.
- [7] Lockhart, R.W., and Martinelli, R.C., 1949, "Proposed Correlation of Data for Isothermal Two-Phase Two-Component Flow in Pipes," *Chem. Eng. Prog.*, **5**, pp. 39-48.
- [8] Chisholm, D., 1967, "A Theoretical Basis for the Lockhart-Martinelli Correlation for Two-Phase Flow," *Int. J. Heat Mass Transfer*, **10**, pp. 1767-1778.